

Segmentation of hepatic artery in multi-phase liver CT using directional dilation and connectivity analysis

Lei Wang^a, Alena-Kathrin Schnurr^b, Yue Zhao^c, Stephan Zidowitz^a, Joachim Georgii^a, Horst K. Hahn^a, Christian Hansen^b

^aFraunhofer MEVIS — Institute for Medical Image Computing, Bremen, Germany

^bComputer-Assisted Surgery Group, University of Magdeburg, Germany

^cCollege of Electronic Science and Engineering, Jilin University, China

ABSTRACT

Segmentation of hepatic arteries in multi-phase computed tomography (CT) images is indispensable in liver surgery planning. During image acquisition, the hepatic artery is enhanced by the injection of contrast agent. The enhanced signals are often not stably acquired due to non-optimal contrast timing. Other vascular structure, such as hepatic vein or portal vein, can be enhanced as well in the arterial phase, which can adversely affect the segmentation results. Furthermore, the arteries might suffer from partial volume effects due to their small diameter. To overcome these difficulties, we propose a framework for robust hepatic artery segmentation requiring a minimal amount of user interaction. First, an efficient multi-scale Hessian-based *vesselness* filter is applied on the artery phase CT image, aiming to enhance vessel structures with specified diameter range. Second, the *vesselness* response is processed using a Bayesian classifier to identify the most probable vessel structures. Considering the *vesselness* filter normally performs not ideally on the vessel bifurcations or the segments corrupted by noise, two vessel-reconnection techniques are proposed. The first technique uses a directional morphological operator to dilate vessel segments along their centerline directions, attempting to fill the gap between broken vascular segments. The second technique analyzes the connectivity of vessel segments and reconnects disconnected segments and branches. Finally, a 3D vessel tree is reconstructed. The algorithm has been evaluated using 18 CT images of the liver. To quantitatively measure the similarities between segmented and reference vessel trees, the skeleton coverage and mean symmetric distance are calculated to quantify the agreement between reference and segmented vessel skeletons, resulting in an average of 0.55 ± 0.27 and 12.7 ± 7.9 mm (mean standard deviation), respectively.

Keywords: Vascular segmentation, liver surgery planning, multi-scale segmentation, directional morphological dilation, Bayesian classification, connectivity analysis

1. INTRODUCTION

According to the data from the GLOBOCAN project, liver cancer is the sixth most common cancer worldwide in 2012¹ and is ranked the second most common cause of cancer deaths. To ensure the sufficient function and survival of the remaining liver tissue after therapy, the supply and drainage of blood as well as the connection to the bile ducts has to be secured. Detailed models of hepatic vein (HV), portal vein (PV), and hepatic artery (HA) are necessary to integrate these conditions into the planning process. Segmentation of these vascular structures is the prerequisite for model construction and computer-assisted surgery planning.

Even though a substantial amount of researches have been conducted on the analysis of vascular structures, it is still considered as an open problem (see 2–4). Hessian-based filters are the major methods used in these efforts so as to enhance tube-like structures but suppress others. Specifically, enhancing tube-like structures is normally based on the analysis of eigenvalues and eigenvectors of the Hessian matrix. A variety of tubular filters have been defined using the ratio of eigenvalues to distinguish tubes from planes and blobs^{5–7}. Manniesing⁸ employed the eigenvalues to define the diffusion tensor of anisotropic filters to enhance vascular structures.

Further author information: (Send correspondence to Lei Wang)

Lei Wang: E-mail:lei.wang@mevis.fraunhofer.de, Telephone: +49 421 218 59293

In addition to eigenvalues, the eigenvectors were also used to develop medialness functions to extract the vascular centerlines.^{9,10} To handle vessels of different radii, a multi-scale framework is usually incorporated in the Hessian-based analysis. The other methods such as the model-based approaches and the level-set techniques were also explored. A directional filter bank was presented by Truc et al. to enhance tubular structures and used 2D images for evaluation.¹¹ Qian et al. defined an enhancement filter based on the probability density function in a polar coordinate.¹² Agam et al. proposed an enhancement filter using the eigenvalues of the correlation matrix of gradient vectors,¹³ while Aylward et al. traced the intensity ridges as the medial axis of tubes.¹⁴ A statistical framework, attempting to estimate a solution vector including the next point on the medial axis, the tangent vector to the next point, and the scale of the tube, was reported by Wong et al.¹⁵ Gulsun et al. proposed a medialness function to look for the medial axis through the minimum-path-cost algorithm.¹⁶ Wörz et al. improved a vascular model for small and large vessels and employed an optimization algorithm to fit the model, find the medial axis, and estimate the radius.¹⁷ Gooya devised a new formulation of level-sets to evolve the front in the longitudinal direction of a tube.¹⁸ In 4, a new filter that enhances medial axis of tubes with a symmetric cross-section was proposed. However, very few works focus on the segmentation of hepatic artery.

In this work, we focus on the segmentation on the hepatic artery. The task is challenging due to the small diameter close to the resolution limit, which might suffer a lot from partial volume effect. Imperfect pre-processing steps, such as the *vesselness* filter, normally generate incomplete initial segmentation of the target vasculature. Hence, the techniques dedicated to fix the vessel tree are demanding. We proposed two vessel-reconnection schemes, attempting to fill the gapped vessel segments and join the missing bifurcations. The entire framework can be easily adapted to segment HV, PV and bile ducts.

2. METHODS

First, a *vesselness* filter on three scales is performed on the input CT volume. The multi-scale *vesselness* response is then further processed using a statistical Bayesian model to identify the most probable vessel structures. Additionally, a directional morphological operator that considers the vessel orientation is performed. After the entry root of the hepatic artery is placed interactively, the connection cost and path to the root are computed for each contiguous artery segment. Finally, the segments are reconnected to one vessel tree. A schematic overview of the entire workflow is illustrated in Fig. 1.

First, a *vesselness* filter on three scales is performed on the input CT volume. The multi-scale *vesselness* response is then further processed using a statistical Bayesian model to identify the most probable vessel structures. Additionally, a directional morphological operator that considers the vessel orientation is performed. After the entry root of the hepatic artery is placed interactively, the connection cost and path to the root are computed for each contiguous artery segment. Finally, the segments are reconnected to one vessel tree. A schematic overview of the entire workflow is illustrated in Fig. 1.

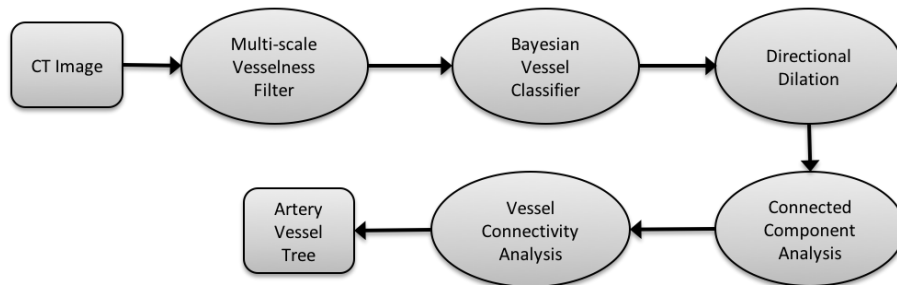


Figure 1. Schematic overview of the entire segmentation workflow.

2.1 Multi-scale vessel enhancement filter

Hessian-based filters have been widely employed to enhance tube-like structures of 3D images. Because the contrast level of HA in different input images is quite heterogeneous, we choose the multi-scale, Hessian-based

vesselness filter introduced by Frangi et al. to enhance artery within the liver mask.⁶ Assuming the eigenvalues of Hessian matrix are sorted in order: $|\lambda_1| \leq |\lambda_2| \leq |\lambda_3|$, the Frangi *vesselness* filter is defined as following:

$$f(\sigma) = \begin{cases} 0 & \text{if } \lambda_2 > 0 \text{ or } \lambda_3 > 0 \\ \left(1 - \exp\left(\frac{-R_A^2}{2\alpha^2}\right)\right) \exp\left(\frac{-R_B^2}{2\beta^2}\right) \left(1 - \exp\left(\frac{-S^2}{2c^2}\right)\right) & \text{otherwise} \end{cases} \quad (1)$$

where

$$R_A = |\lambda_2|/|\lambda_3|, \quad R_B = \frac{|\lambda_1|}{\sqrt{|\lambda_2\lambda_3|}}$$

and

$$S = \sqrt{\lambda_1^2 + \lambda_2^2 + \lambda_3^2}.$$

The ratio R_A is designed to differentiate vessels from sheet-like structures, whereas R_B is used to distinguish vessels from blob-like structures. The term S aims to suppress noise structures. The scale parameter σ indicates the size of Gaussian kernel used for calculating Hessian matrix. The parameters used in this filter, α, β and c are set to 0.5, 0.5 and 10. Considering the radius range of HA, we choose three optimized scales for σ : 1 mm, 1.2 mm, and 1.4 mm based on our experimental tests, which are able to capture vessels with thin, medium, and thick radii. The ultimate *vesselness* response is obtained by extracting the maximum across all scales.

2.2 Bayesian vessel classifier

The *vesselness* outputs of three scales are individually assessed with a Bayesian vessel classifier that uses a Gaussian mixture model (GMM), assuming that the image is a mixture of a finite number of Gaussian distributions with unknown parameters. The Bayesian vessel classifier is supposed to differentiate the vasculature from non-vasculature based on the *vesselness* response. Therefore, the number of Gaussian distributions in the GMM is assumed as two. The expectation maximization (EM) algorithm is exploited to estimate the mean and the variance of each Gaussian distribution. Since the EM algorithm requires initializing all parameters, mean, variance and probability for both classes have to be estimated. The Frangi's *vesselness* measurement is comparable across scales and images, which makes it possible to determine a set of initial parameters. To further simplify the process, a minimal *vesselness* threshold was used to discard background voxels with close to zero *vesselness* response. Using the parameters calculated by the EM algorithm, the probability distribution of vasculature and non-vasculature classes are achieved. Thus, a voxel belonging to a class c based on its *vesselness* value x can be obtained using Bayesian formula: .

$$p(c|x) = (p(x|c) \times p(c))/p(x) \quad (2)$$

Each voxel is then assigned to the class with higher probability. This classification is conducted for all three *vesselness* outputs. A voxel is marked as vessel in a binary output image (as shown in Fig. 2 (b)), if it is classified as vessel in one of the three scales.

2.3 Directional morphological dilation

The binary output of the Bayesian vessel classifier depicts the most probable vessel segments with gaps and holes. To close small gaps in between and also fill holes, a directional morphological dilation along the vessel orientation is applied.

Although dilation is a common used morphological operator to fill the gap in binary images, it often merges irrelevant neighboring structures. To overcome this problem, the orientation of a vessel segment, which is derived from the eigenvector of the hessian matrix that correlates to the smallest eigenvalue, is incorporated in the dilation process. The structure element is defined as a line with a fixed length along the local vessel orientation (see Fig. 2(a)). The directional dilation performs only on the background voxels near to the detected vessel segments. The voxel values of the line element are interpolated. The percentage of foreground voxels is computed and compared to a percentage threshold. If the percentage exceeds the threshold, the currently processed background voxel is labeled as foreground in the output image. To achieve a higher level of connectivity, this dilation procedure is performed twice. The second round utilizes the result of the first round as the input. Compared with the vessel segments identified by Bayesian classifier (see Fig. 2(b)), the dilated vessel segments as depicted in Fig. 2(c) tend to be more connected with fewer gaps.

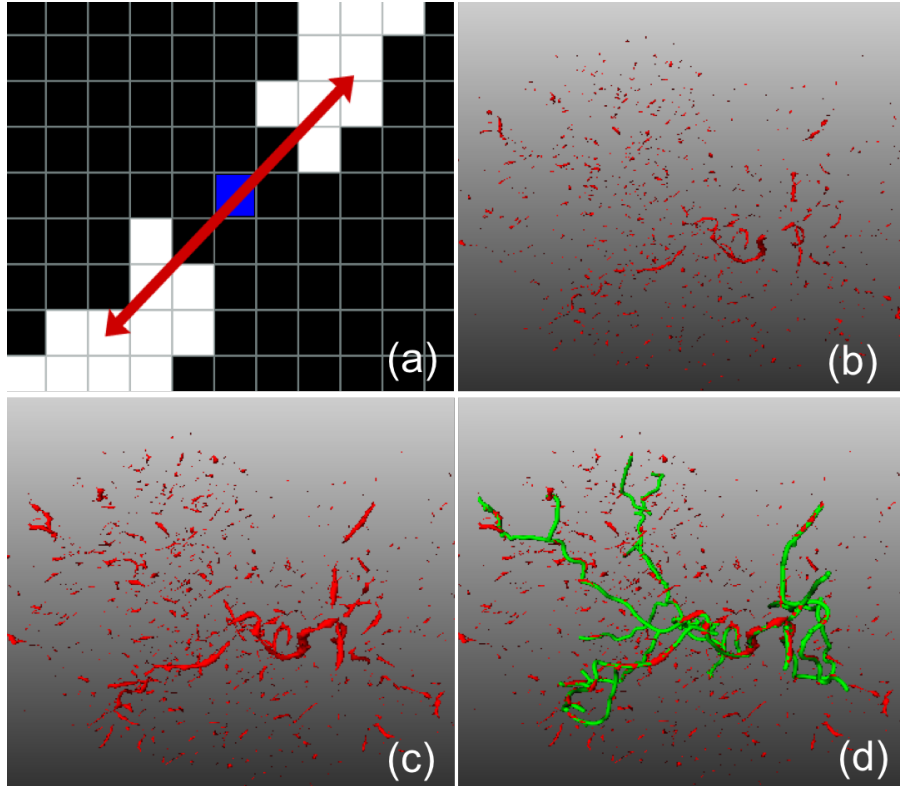


Figure 2. (a) directional dilation kernel (red line) applied in a background voxel (blue); (b) vessel segments resulted from Bayesian classifier; (c) vessel segments resulted from directional dilation; (d) the reconstructed HA vessel tree (green) obtained by connecting and merging vessel segments.

2.4 Vessel connectivity analysis

To some extent, the directional dilation shows its ability to bridge the gaps between vessel segments, but still does not work well enough to build a complete HA vessel tree. Particularly, the bifurcations connecting different level of branches can be missing, due to the inherent weakness of the *vesselness* filter, which normally performs imperfectly in joint regions. To build a complete vessel tree, a root is required to be identified, and the connectivity of all vessel segments to their parent branches, and ultimately to the root needs to be analyzed. We analyze the vessel connectivity by computing the cost of the path connecting a vessel segment to the root, which consists of several steps.

2.4.1 Skeleton components extraction

First, a connected component analysis is performed on the skeletons of the dilated vessel segments. The skeleton, representing the centerline voxels of a vessel segment, is extracted by a thinning operation. A component is defined as a group of skeleton voxels and has a unique index. The size of a component is the number of its skeleton voxels. The radius and the 3D position of each skeleton voxel are saved. All vessel segments are traversed, and their corresponding components are constructed. Not all components will be fed to the subsequent steps, and a valid component should fulfill two conditions:

- its size should be larger than a minimum threshold
- it should not form a ring structure.

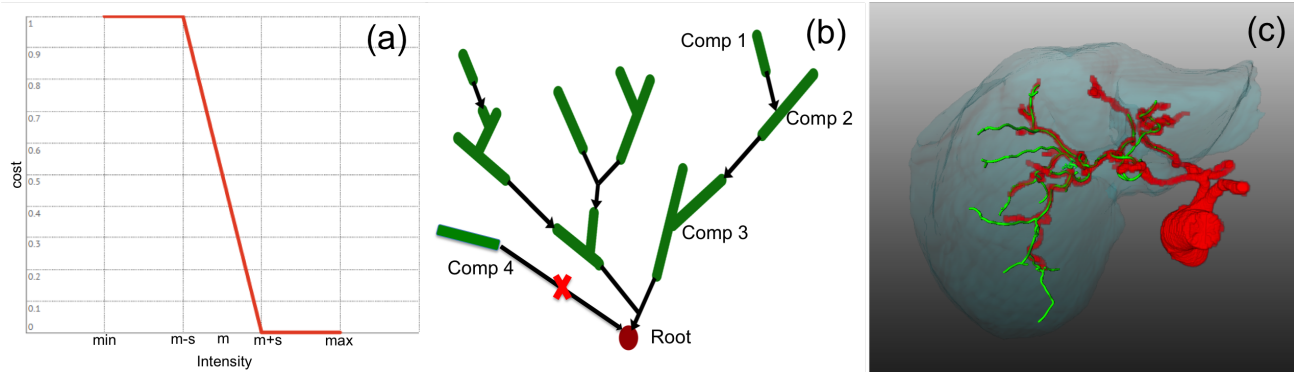


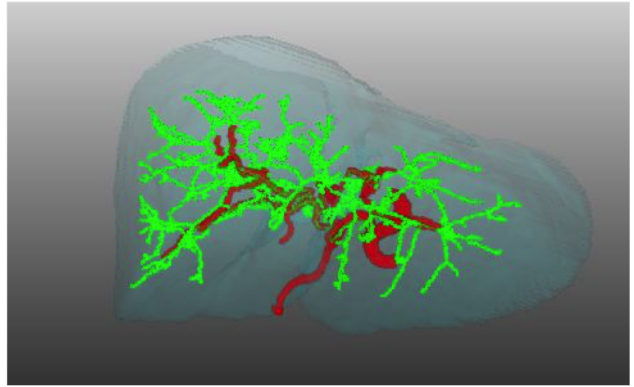
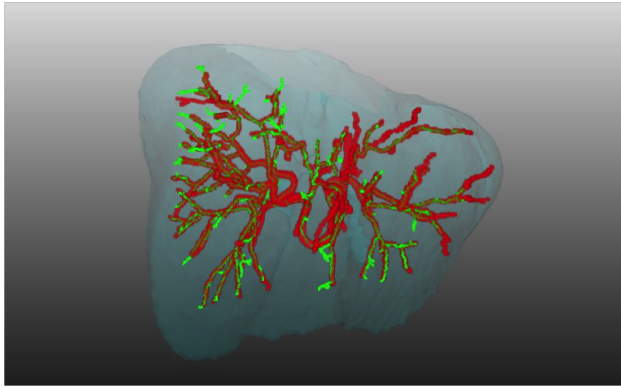
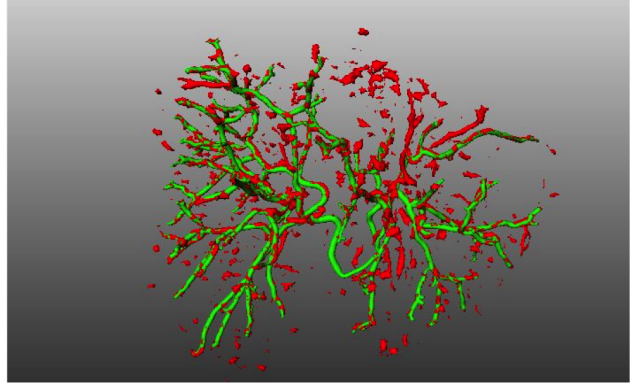
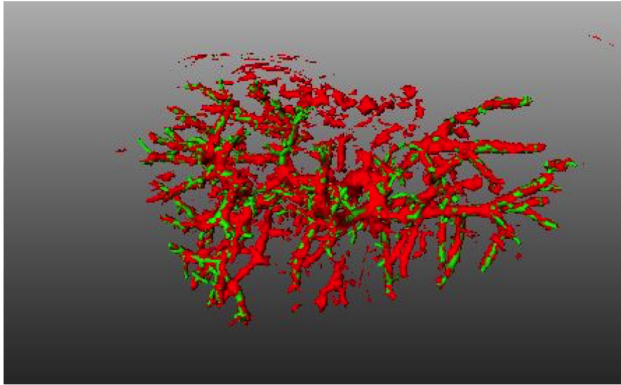
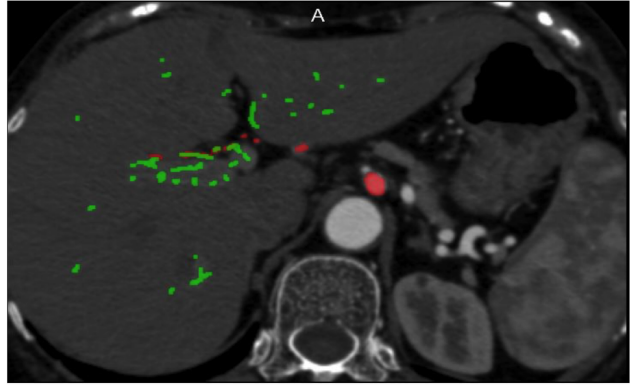
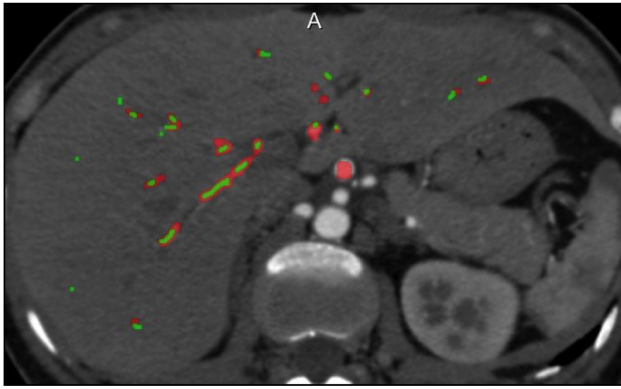
Figure 3. (a) Mapping function to compute the cost image; (b) illustration of optimal path from components to the root and the connection cost (arrow length is proportional to the cost strength) between primary component (such as Comp 1) to its follower (Comp 2). Comp 4 will not be reconnected to the root due to the cost exceeding the threshold; (c) 3D visualization of reference HA volume (red) and segmented HA skeleton (green).

2.4.2 Connection cost computation

The HA vessel system is assumed to be a tree structure with a root node that can be selected as any point on the main HA branch, before it further splits to small branches in the liver. Considering the HA anatomy, the root may be defined either inside or outside the liver. To ensure the accuracy of the root position, it was decided to place the root by the user interactively. To calculate the connection cost from a skeleton component to the root, a cost image has to be built. We generate a cost image by applying a transfer function on the intensities of the original CT image as depicted in Fig. 3(a). First, the mean (m) and standard deviation (s) of the intensities are calculated. The function maps all the intensities smaller than $m - s$ to 1 and all the ones larger than $m + s$ to 0. The intensities in between will be mapped linearly to the range of (0, 1). Additionally, the cost value of all skeleton voxels in each component is set to 0. Then, the Dijkstra algorithm is applied on the cost image, and the optimal path with the minimal cost from any voxel to the root can be found. Because the cost traveling from one skeleton voxel to another within a component is 0, the voxels belonging to the same component will result in the same optimal path. This path is then defined as the optimal path for the component to reach the root, and the corresponding connection cost is the sum of the cost values along the path.

2.4.3 Vessel component connecting

After the optimal paths to the root for all the components have been found, the component connecting process is triggered. First of all, two additional attributes are assigned to each component: the follower and the cost to the follower. For a primary component, its optimal path is traced towards the root. If another component is found on the path, the tracing process stops. The found component is assigned as the follower for the primary one, and the cost between them is the subtraction of their costs to the root. Certainly, it is possible that no other component is found on the optimal path till the root, and then the follower for the primary component is set as the root and the cost to the follower is identical as the cost to the root. Afterwards, the costs to the follower for all components are sorted in ascending order. The component connecting and merging process is started with the one with the minimal cost and iterate through all the components based on the cost order. To avoid unreliable connecting, the primary component and its follower will be connected and merged only if the cost is under a threshold. For the components of which the followers are the root, the cost threshold is doubled, because the root might be placed a little bit far from the liver arising higher cost. The entire process is illustrated in Fig. 3(b). The gap between a primary component and its follower is filled with the skeleton voxels on the optimal path. The radii of these skeleton voxels are interpolated with the radii of the primary and the follower component voxels. Finally, all connected and merged components that can reach the root are selected to build the complete HA vessel tree, which serves as the segmentation results as shown in Fig. 3(c).



Case Nr. 14
SC = 0.88

Case Nr. 16
SC = 0.08

Figure 4. Examples showing two cases with high (left column) and low (right column) SC values. (Top row) the 2D view of ground truth (red) and segmentation (green); (Middle row) the vessel segments (red) and the reconnected vessel branches (green); (Bottom row) the 3D visualization of ground truth (red) and segmentation (green).

3. RESULTS

3.1 Data sets

We collected 18 hepatic multi-phase CT datasets with tumors for the evaluation of our approach. All data sets have a voxel spacing of $0.7\text{mm} \times 0.7\text{mm} \times 0.8\text{mm}$. For each dataset, the liver was imaged once in the venous phase and once in the arterial phase. The liver mask and HA vessel were segmented manually by a medical professional (MeVis Distant Service, Bremen, Germany), and the latter serves as the reference for evaluation. The similarity of two vessel trees is difficult to express with a single measurement. Regarding the time efficiency, processing one dataset overall took about 1 minute on average on a machine with a 6-Core 3.5 GHz CPU, in which about 5 seconds were taken to place the root interactively.

3.2 Evaluation metrics

The error of misalignment can result from two sources: branching pattern and radius, which need to be addressed with different measurements. To assess the quantitative segmentation quality, the following metrics were used:

- Skeleton coverage (SC): percentage of the segmented skeleton covered by the reference vessel volume
- Mean symmetrical distance (MSD): mean distance between the segmented and reference skeletons

If the branching pattern of the segmentation is accurate, its skeleton should be completely covered by the reference volume, resulting in a higher SC value. MSD is even more sensitive to the error of branching patterns. These metrics were computed inside the liver mask. The mean and standard deviation values of SC and MSD were 0.55 ± 0.27 and $12.7 \pm 7.9\text{mm}$, respectively. Figure 4 demonstrates two example cases with relatively high and low SC values. It can be observed that the algorithm is capable of capturing the majority of enhanced HA vessels which are enhanced properly with a significant contrast with surroundings. On the other hand, in the cases where the segmentation performs not well, normally HV and PV vasculatures are substantially enhanced as well, due to imperfect imaging time during the acquisition. If the HA phase is taken imperfectly with enormous enhancement of other vasculatures such as HV and PV, the algorithm can be misled and generate a substantial amount of false positive segmentation. Additionally, as shown in Fig. 3(c), the manually annotated reference often did not reach the small HA branches deep inside the liver. Some more examples visually depicting the performance are given in Fig. 5.

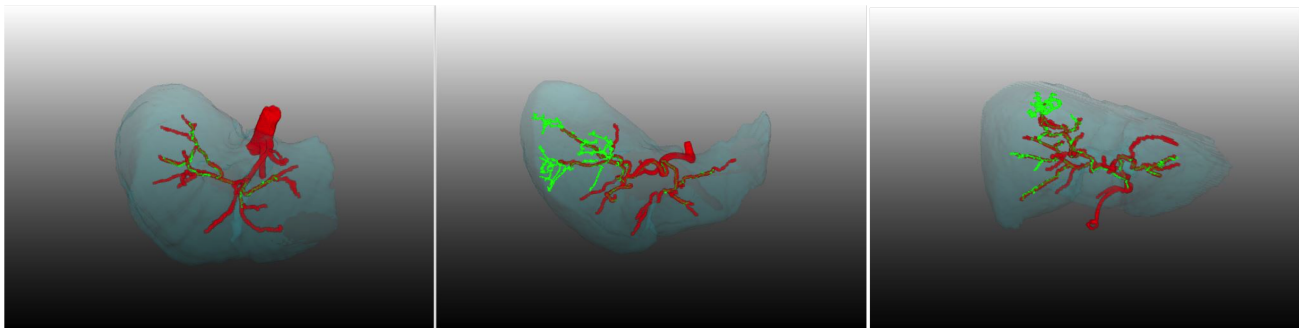


Figure 5. Visual demonstration of the reference (red) and segmented (green) HA vessels.

4. CONCLUSIONS AND DISCUSSIONS

In this work, we developed a framework dedicated to hepatic artery segmentation in CT for liver surgery planning. The proposed directional dilation morphological operator along the vessel centerline orientation is capable of bridging the gap between the broken vessel segments to some extent. The subsequent Dijkstra-based vessel connectivity algorithm has a great potential to reliably reconstruct the complete vessel tree, and thus to improve the workflow of liver surgery planning. To guarantee the performance of the algorithm, the HA phase CT should be taken with a satisfactory quality where no substantial amount of other vasculatures are enhanced.

REFERENCES

- [1] Ferlay, J., Soerjomataram, I., Dikshit, R., Eser, S., Mathers, C., Rebelo, M., Parkin, D. M., Forman, D., and Bray, F., “Cancer incidence and mortality worldwide: Sources, methods and major patterns in GLOBOCAN 2012,” **136**(5), E359—E386 (2015).
- [2] Kirbas, C. Quek, F., “A review of vessel extraction techniques and algorithms,” *Computing Surveys* **36**(2), 81–121 (2004).
- [3] Lesage, D., Angelini, E. D., Bloch, I., and Funka-Lea, G., “A review of 3D vessel lumen segmentation techniques: models, features and extraction schemes.,” *Medical image analysis* **13**, 819–45 (Dec. 2009).
- [4] Foruzan, A. H., Zoroofi, R. a., Sato, Y., and Hori, M., “A Hessian-based filter for vascular segmentation of noisy hepatic CT scans,” *International Journal of Computer Assisted Radiology and Surgery* **7**, 199–205 (Mar. 2012).
- [5] Sato, Y., Nakajima, S., Shiraga, N., Atsumi, H., Yoshida, S., Koller, T., Gerig, G., and Kikinis, R., “Three-dimensional multi-scale line filter for segmentation and visualization of curvilinear structures in medical images.,” *Medical image analysis* **2**, 143–168 (June 1998).
- [6] Frangi, A. F., Niessen, W. J., Vincken, K. L., and Viergever, M. a., “Multiscale vessel enhancement filtering,” in [*Medical Image Computing and Computer-Assisted Intervention - MICCAI’98. Lecture Notes in Computer Science, vol 1496*], **1496**, 130–137, Springer (1998).
- [7] Kawajiri, S., Zhou, X., Zhang, X., Hara, T., Fujita, H., Yokoyama, R., Kondo, H., Kanematsu, M., and Hoshi, H., “Automated segmentation of hepatic vessels in non-contrast X-ray CT images.,” *Radiological physics and technology* **1**, 214–22 (July 2008).
- [8] Manniesing, R., Viergever, M. a., and Niessen, W. J., “Vessel enhancing diffusion. A scale space representation of vessel structures,” *Medical Image Analysis* **10**(2006), 815–825 (2006).
- [9] Krissian, K., Malandain, G., and Ayache, N., “Model based multiscale detection and reconstruction of 3D vessels,” *Sophia* (1998).
- [10] Pock, T., Janko, C., Beichel, R., and Bischof, H., “Multiscale Medialness for Robust Segmentation of Method Detection of Tubular Structures,” in [*10th computer vision winter workshop*], (2004).
- [11] Truc, P. T. H., Khan, M. a. U., Lee, Y. K., Lee, S., and Kim, T. S., “Vessel enhancement filter using directional filter bank,” *Computer Vision and Image Understanding* **113**(1), 101–112 (2009).
- [12] Qian, X., Brennan, M. P., Dione, D. P., Dobrucki, W. L., Jackowski, M. P., Breuer, C. K., Sinusas, A. J., and Papademetris, X., “A non-parametric vessel detection method for complex vascular structures.,” *Medical image analysis* **13**, 49–61 (Feb. 2009).
- [13] Agam, G., Armato, S. G., and Wu, C., “Vessel tree reconstruction in thoracic CT scans with application to nodule detection,” *IEEE Transactions on Medical Imaging* **24**(April), 486–499 (2005).
- [14] Aylward, S. R. and Bullitt, E., “Initialization, noise, singularities, and scale in height ridge traversal for tubular object centerline extraction,” *IEEE Transactions on Medical Imaging* **21**(February), 61–75 (2002).
- [15] Wong, W. C. K. and Chung, a. C. S., “Probabilistic vessel axis tracing and its application to vessel segmentation with stream surfaces and minimum cost paths,” *Medical Image Analysis* **11**(2007), 567–587 (2007).
- [16] Gulsun, M. A. and Tek, H. T. H., “Geometric modeling of tubular structures,” *2008 IEEE Computer Society Conference on Computer Vision and Pattern Recognition Workshops* (2008).
- [17] Wörz, S. and Rohr, K., “Segmentation and quantification of human vessels using a 3-D cylindrical intensity model.,” *IEEE transactions on image processing : a publication of the IEEE Signal Processing Society* **16**, 1994–2004 (Aug. 2007).
- [18] Gooya, A., Liao, H., Matsumiya, K., Masamune, K., Masutani, Y., and Dohi, T., “A variational method for geometric regularization of vascular segmentation in medical images,” *IEEE Transactions on Image Processing* **17**(August), 1295–1312 (2008).